SOLAR CADASTER IN URBAN AREA INCLUDING VERTICALITY

Karine Bouty[1], Leon Gaillard[1], Martin Thebault[1], Ismaël Lokhat[2], Aurélien Gallice[2] and Christophe Ménézo[1]

[1] LOCIE UMR CNRS/USMB, Institut National de l'Energie Solaire, 73376 Le Bourget-Du-Lac cedex – France

[2] Cythelia Energy, la Maison ZEN, 350 Route de la Traverse, 73000 Montagnole

Abstract

Solar cadasters, have been mainly focusing on the prediction of the solar potential on roofs. However, in dense urban areas there is sometimes most solar potential to be collected from vertical surfaces than from the roofs. Not sufficient assessment for economical and urban energy planning. Possibility of shorter and dynamical time period simulation has to be accessible. Moreover, in comparison with roof, building facades are representing big potential for solar PV integration even if inclination is not optimal. Archelios map® developed by Cythelia Energy is used to generate a solar cadaster, which can then be incorporated into the local authority's geographic information system (GIS) and/or uploaded to its website. For now, Archelios map® takes into account the brute solar radiation on tilted rooftops (only, not facades). It takes into account tilt and orientation. The main objective is to extend the actual cadaster features so it gives a solar cadaster including solar potential on facades by considering the inter buildings effect and the urban environment climate so we can increase the solar power generation.

Keywords: Solar cadaster, solar power potential, roof and façade, local climate, solar reflected radiation.

1. Introduction

With the increase of the urban population, cities represent areas of high electrical power needs but low production. Solar power represents on abundant well distributed renewable source of energy and can moreover be used to generate different type of energy. As a result, the calculation of the solar potential becomes more and more important in order to plan Photovoltaic (PV) integration in urban environment. The calculation of the solar potential in an urban city gives an idea of the solar potential of each building. The solar potential of a building depends on different parameters among them one can cite the local irradiation, the orientation and the tilt of the solar system or the local operating conditions. Several studies have been done on how to get the most out of the solar potential by focusing on the positioning method of the PVs. According to the literature, for optimal orientation of PV, the solar radiation is increasing by 4% compared to the fixed annual orientation (Al Garni, Awasthi, et Wright 2019). This value decreases when considering an urban context.

A solar cadaster offers many advantages for city. If it is based on a 3D description, it provides orientation, angle, irradiation, and the potential of solar production for each building envelope. Most solar cadasters takes into consideration horizontal surfaces in the calculation of the solar potential (Yuan et al. 2016). The consideration of the vertical surfaces, also called facades, have an important effect on the solar potential predictions. The study of solar energy potential done by (Redweik, Catita, et Brito 2013), shows that the irradiation reaching facades is smaller than that of the roofs, but while working with big areas, facades have an important impact on the solar potential of buildings in an urban area. As well as (Brito et al. 2017) who proved that during winter, facades have the potential to double the solar potential, due to the more favorable inclination. Furthermore, the reflected rays between buildings are neglected in the calculation of solar radiation, (Lobaccaro et al. 2012) highlighted the effect of these rays in the urban region.

In an urban area, solar power potential, include several constraints (Naboni et al. 2019). It is the case of vegetation (green space), thermal effects (Morakinyo, Balogun, et Adegun 2013), the spacing between the buildings and the different components of radiation (direct, diffuse and reflected)... The morphology of urban region plays an important role in estimating solar production as shown by (Zhang et al. 2019). In addition to that, temperature can

doi:10.18086/swc.2019.45.01 Available at http://proceedings.ises.org

change the potential of PV panels and it is therefore necessary to take into account urban heat island phenomena while the calculation of solar potential in urban region (Bloem 2008).

The work presented here is a numerical study, of solar radiation in order to know the role of the reflected radiation and the shading in the calculation of solar potential. Two cases studies are investigated, one corresponding to a simple ordered geometry and the second to a part of the district of Carouge in Geneva.

2. Numerical methodology

2.1 Solar radiation theory and modelling

The solar radiation reaching a surface generally subsists of three components, direct, diffuse and reflected. The direct, or beam, solar radiation is that received from the sun without having been interrupted by the atmosphere. The direct solar flux reaching a surface is symbolized by ID. If the surface is perpendicular to the solar rays, the incident solar flux is equal to the Direct Normal flux, IDN. The direct solar flux arriving to the surface is obtained by:

$$I_D = I_{DN} \cos\theta \qquad \text{(eq.1)}$$

where θ is the angle of incidence. The diffuse solar radiation is that received from the sun after changing direction because of an obstacle. Diffuse radiation falling on a surface is noted as Id while it is notedI_{dH} when achieving horizontal surface. The diffuse radiation is hard to compute because of its no directional nature. The latter is expressed, considering that the sky is a diffuse source, by the following equation:

$$\frac{I_d}{I_{dH}} = (1 + \cos\Sigma)/2 \qquad \text{(eq.2)}$$

Where Σ is the surface tilt angle. The reflected solar radiation it is the part that falls on a surface after touching another surrounding surfaces. This component depends on the geography of the area, the orientation and the reflective characteristics of the surrounding surfaces. It's noted by I_R given by the equation 3:

$$I_R = \rho_g I_H (1 - cos\,\Sigma)/2 \qquad \text{(eq.3)}$$

Where: ρ_g = solar reflectance of the ground and I_H = Total solar flux reaching the horizontal ground

The total solar flux I attaining a surface at any time is the sum of the three components:

$$I = I_d + I_R + I_D \qquad \text{(eq.4)}$$

Diffuse hourly irradiation on an inclined surface$I_{d\beta}$:

As a general rule, diffuse radiation models for inclined surfaces can be classified into two groups: isotropic and anisotropic models. They are differentiated by the division of the sky into normal regions and high diffuse radiation intensities. Isotropic models assume uniformity in the distribution of diffuse radiation intensity over the sky. Anisotropic models include modules suitable for representing areas of high diffuse radiation.

1. Anisotropic

The Perez model is an anisotropic sky model, the total of diffuse energy according to these three parameters (the sky, the circumsolar and the horizon) is calculated by the following equation:

$$I_{d\beta} = I_d \left[(1 - F_1) \left(\frac{1+cos\,\beta}{2} \right) + F_1 \frac{a}{b} + F_2\, sin\,\beta \right] \qquad \text{(eq.5)}$$

Thus, the model will operate both in an isotropic configuration (F1 = F2 = 1) and will collectively incorporate circumsolar equivalent time and / or horizon lightening. Where F_1 is the brightness coefficient of the sky, $F_2$the brightness of the horizon, I_d diffuse irradiation using weather file (kwh), a and b are related to the visibility and then the angles of geometry and are calculated by the following equations

$$a = \max(0, \cos\theta) \qquad \text{(eq.6)}$$

$$b = max(\cos 85\,, \cos\theta_z) \qquad \text{(eq.7)}$$

$\left(\frac{1+\cos\beta}{2}\right)$ represent the sky view factor

An anisotropic sky is usually related to climatic conditions that are uniformly distributed in the sky. Then Perez et al. They found that relative to a ground surface, the luminosity changes over the entire surface of the sky and so they computed luminosity factors statistically (Perez, Seals, et Michalsky, s. d.) that allows defining the anisotropic relationship. And as a result the brightness factor present in the equation of calculation of the total diffuse energy (Eq. 5) is then calculate by the equations below:

$$F_1 = max\left[0.\left(f_{11} + f_{12}\Delta + \frac{\pi\theta_z}{180} f_{13}\right)\right] \quad \text{(eq.8)}$$

$$F_2 = \left[\left(f_{12} + f_{22}\Delta + \frac{\pi\theta_z}{180} f_{23}\right)\right] \quad \text{(eq.9)}$$

Where Δ is the brightness parameter;

$$\Delta = m\,\frac{I_d}{I_o} \quad \text{(eq.10)}$$

Where m is the mass of air given by equation 11 and I_o the extraterrestrial irradiation given by equation 12.

$$m = \frac{1}{cos\,\theta_z} \quad \text{(eq.11)}$$

$$I_o = 1367\left(1 + 0.033\cos\frac{360n}{365}\right) \quad \text{(eq.12)}$$

Another anisotropic model is that proposed by Hay and Davies, commonly called Hay model. Two main sources are supposed to be the origins of the diffuse radiation of the sky, namely the disk of the solar disk and the rest of the sky with diffuse isotropic radiation (Hay 1979). The two components are described by the anisotropy index f_{Hay}:

$$f_{Hay} = \frac{I_b}{I_o} = \frac{I_H - I_d}{I_o} \quad \text{(eq.13)}$$

According to Hay's model, the equation of diffuse irradiance intensity on an inclined surface is:

$$I_{d\beta} = I_d\left[f_{Hay}\left(\frac{\cos\theta}{\cos\theta_z}\right) + \left(\frac{1+\cos\beta}{2}\right)\left(1 - f_{Hay}\right)\right] \quad \text{(eq.14)}$$

2. Isotropic

Badescu presented a model of diffuse solar radiation on a sloping surface using the following elements (Badescu 2002):

$$I_{d\beta} = \left(\frac{3+\cos(2\beta)}{4}\right) I_d \quad \text{(eq.15)}$$

- Liu and Jordan's model is one of the oldest and simplest radiation models (Liu et Jordan 1960). This model assumes that the intensity of diffuse radiation is uniformly distributed over the entire sky, which is calculated as follows:

$$I_{d\beta} = \left(\frac{1+\cos\beta}{2}\right) I_d \quad \text{(eq.16)}$$

2.2 Geometry and solar radiation modelling

Solar potential analyses are usually simulated on 2.5 D models, such as roof surfaces (Desthieux et al. 2018). When applying 3D models methods, it allows the simulation of solar radiation on all building surfaces also accounting for inter-reflections. A lot of software are able to perform calculations of solar radiation on horizontal surfaces, so we must choose one that gives more precision regarding reflected ray-modeling and allows performing more studies on vertical surfaces (facades).

- EnergyPlus® is a software that allows doing a solar radiation calculation on building. It is however

limited by the precision in level of reflected radiations and in addition, the calculation of solar radiation is performed for one chosen building taking into consideration the effects of the neighboring buildings.

- Radiance® is a tool that applies Perez's model of diffuse radiation and considers diffused and reflected radiations in urban environment. This software uses ray-tracing and light-backwards algorithms based on the physical behavior of light in a 3D volumetric model. It is a validated software and very well used in applications related to the estimation of the solar potential on the roofs of buildings and facades for the production of electricity and the analysis of daylight. DIVA-for-Rhino® is a highly optimized plug-in for modeling daylight and energy for the Rhinoceros model. It allows users to perform a series of assessments of the environmental performance of individual buildings and cityscapes, including radiation maps, realistic photo rendering, and climate-based daylighting. A glare analysis in annual and individual time steps, daylight compliance and energy calculations of a single thermal zone. DIVA-for-Rhino comes with an improved user interface: Grasshopper®. Drop-down settings allow to quickly select materials. Input and output parameters can be added and removed from components in one click, allowing full control of script complexity. Grasshopper is a modeling algorithmic plugin for Rhino that uses a visual programming language. It is a parametric design tool. Programs are created by dragging components onto a canvas. The outputs of these components are then connected to the inputs of the following components. DIVA-for-Rhino utilize Radiance in order to calculate solar radiation on buildings.

For RADIANCE software The lighting simulation engine uses a hybrid approach of Monte Carlo and deterministic ray tracing to achieve a reasonably accurate result in a reasonable time. The method employed starts at a measurement point (usually a viewpoint) and traces rays of light backwards to the sources (ie. emitters). The calculation can be divided into three main parts: the direct component, the specular indirect component, and the diffuse indirect component. DIVA-FOR-RHINO generate the irradiation map using RADIANCE, it is possible to vary a given number of Radiance parameters. From these parameters we note –ab parameter: the number of ambient bounces to N. This is the maximum number of diffuse bounces computed by the indirect calculation. A value of zero implies no indirect calculation. By increasing the number of ambient bounces, we achieve more precision in calculation of solar radiation concerning reflected rays.

2.3 Urban weather generator (UWG)

As mentioned in the introduction, temperature impacts the PV production and it is therefore necessary to evaluate the local temperature to provide more accurate solar potential prediction. To that aim an urban weather generator, developed by (Bueno et al. 2014) is used. UWG calculates the hourly values of urban air temperature and humidity based on reference weather data typically measured outside a city. It requires an EnergyPlus weather (epw) file and an Extensible Markup Language (xml) file describing the urban and rural site characteristics.

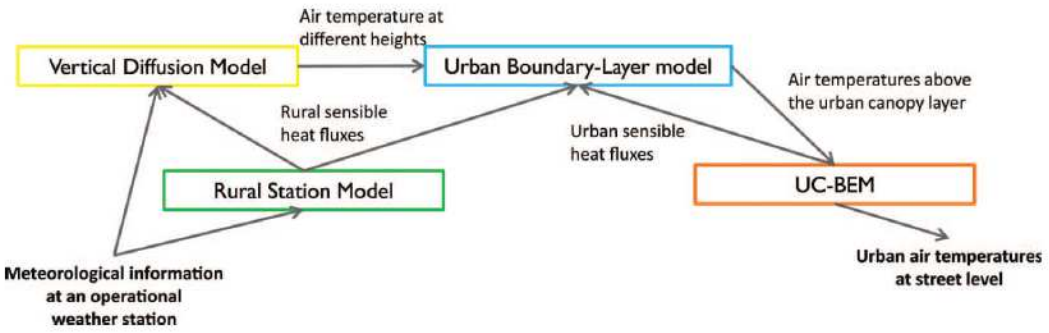

Figure 1: UWG principal of calculation

3. Cases of study

The objective of the study is to estimate solar potential in urban areas, taking into consideration the different constraints. The work will allow considering the geometry of the district and its microclimate (inter building effects, diffused and reflected radiation, wind, vegetation, urban heat island). So we can optimize the solar energy power generation. In addition to that, vertical surfaces are to taken into consideration. In order to properly consider the inter-building effect in the calculation of solar potential, we first focus on the reflected radiation from obstacles surrounding the buildings. To illustrate the role of reflected radiation, as well as the role of obstacles, several tests are performed on urban district morphology using Rhino-for-Diva.

Two cases studied will be considered. The first case corresponds to the simple one, shown in Figures 2 and 3, represent a study of solar potential for the roof of a building surrounded by several buildings, compared then by adding a new partially reflective obstacle.

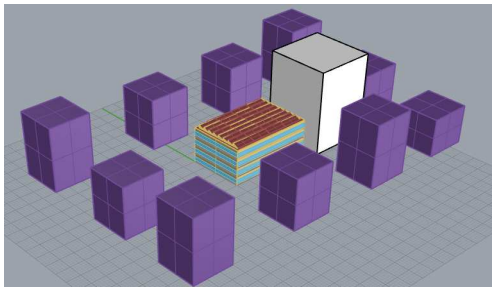

Figure 2: Adding a long building next to the target house.

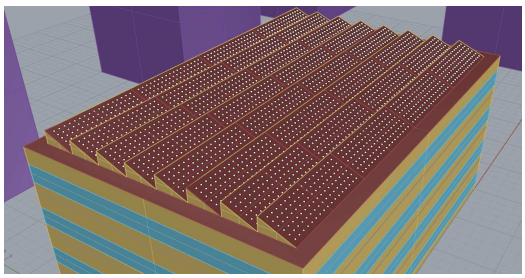

Figure 3: studied surface divided by 102 nodes / module

The second case of study is applied to a real neighborhood in Geneva. This case study aims to visualize the effect of the reflectivity of building materials in the calculation of solar potential. Figure 4 shows the 3D data of the neighborhood in Geneva. Diva-for-rhino is used with the Geneva's weather file, to obtain visualizations of irradiation maps by changing the properties of the surface materials of the building in the whole district. Two simulations are performed simultaneously with:

o 90% reflective materials

o 35% reflective materials

The simulations are done using a low quality so for an ambiance bound equal two, so we can optimize the simulation time.

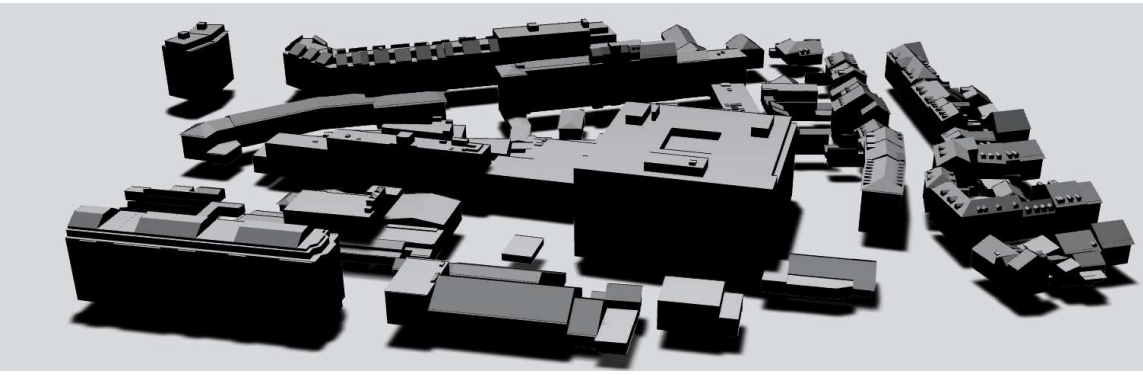

Figure 4:Geneva area to study.

4. Results

- Case1: The studied surface is divided by 102 nodes / module (32 modules in total):

The results for these case of study are generated using DAYSIM integrated into DIVA. The results obtained make it possible to have for a year and every hour the irradiation value. In our case, for the easy visualization of the

results, the results are generated with the irradiation data, for a most critical PV module and therefore for the one closest to the addition obstacle: PV8. Figure 5 shows respectively the annual irradiation map of the studied surface, with the addition of the reflecting obstacle and without the addition, zoomed on the modules 4, 8, 12 and 16. Each node represents an irradiation value in kWh / m2 represented by color: the darker the colour is and the closer is to red, the higher is the irradiation. This range of irradiation normally depends on location, geography and building materials and it will result a different value if it was done at equator. In total 32 modules are studied, each module is meshed in 102 nodes to have a more detailed idea of irradiation arriving on the total studied surface. Simulations are done for an ambiance bounces equal to 2 and for a start time at 01/01 and an end time at 31/12 for 00: 24 range of time.

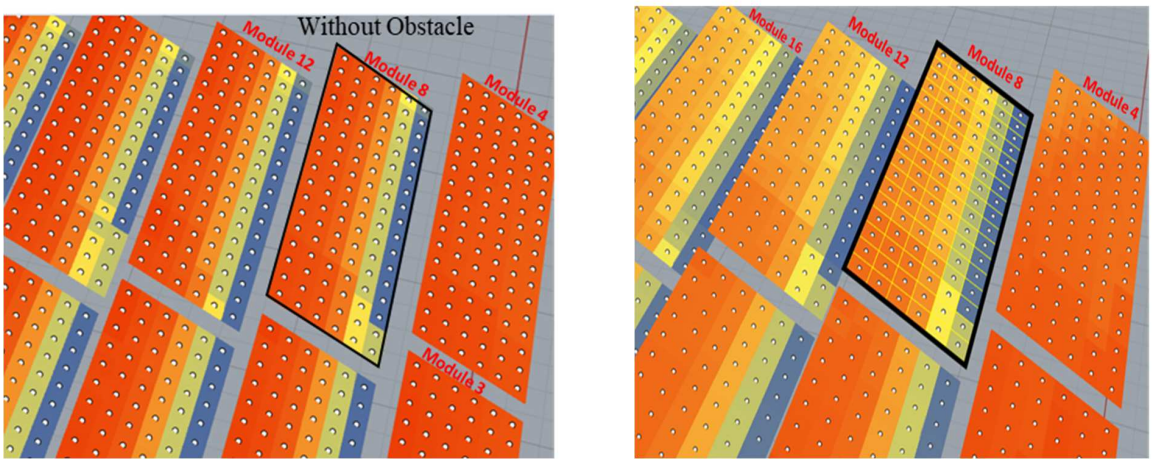

Figure 5: Annual field of intensity of incident solar radiation with and without obstacle.

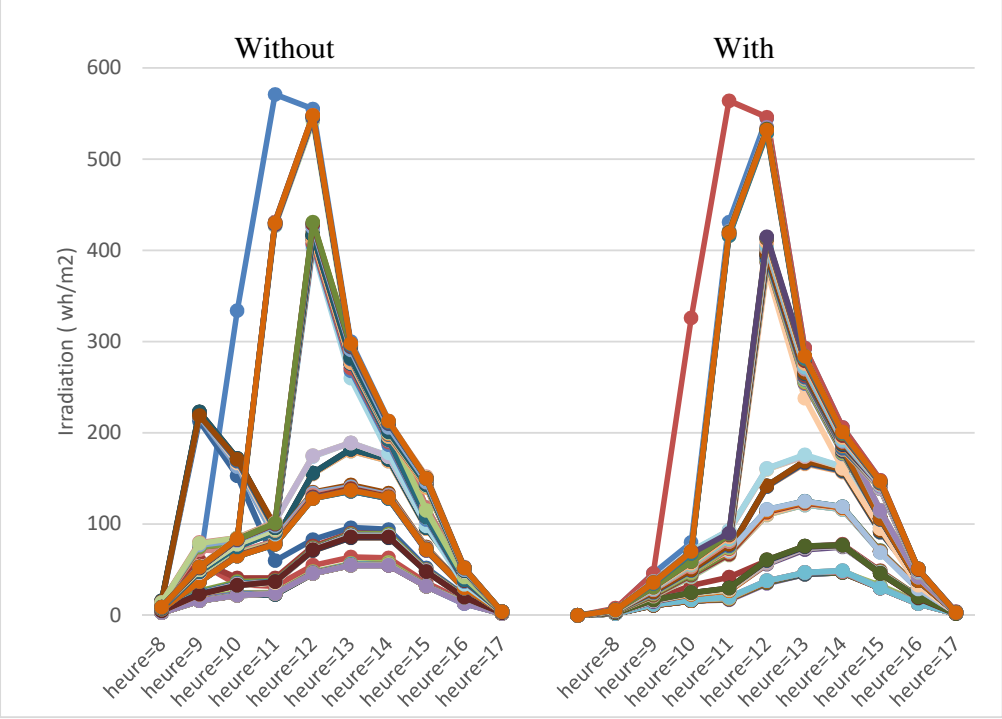

Figure 6: Hourly irradiation per node on the PV module 8 (without and with obstacle) for the first of January.

Figure 6 represents the irradiation hourly simulation results on the PV8 module (102 node). This graph shows a comparison between the irradiation received between 8am in the morning and 17h in the evening without and with the addition of the obstacle for the first of January. The left graph shows this values of irradiation for the studied surface and the one at right, the values after adding the obstacle. In total, 102 curves, each one represents the hourly irradiation for one node. The addition of a non-reflecting obstacle, contributes to the decrease of the irradiation arriving at the studied surface especially between 8am and 11 in the morning. This is obvious cause when adding an obstacle, it shades on other building and so the quantity of radiation decrease. To evaluate this change of irradiation on the studied surface, total hourly irradiation (between 7 am and 15 pm) on the first 16 PV modules, for first of January, is calculated by adding all the irradiation received on the 102 notes of each module and represented in form of two tables: one with obstacle in table 1 and the other without. As shown in the two tables, the modules 4,12 and 16, therefore the ones closest to the addition of the obstacle, are the modules most affected in terms of the decrease of solar radiation (by 6 to 50%). For the modules farthest from the obstacle there is a slight decrease (about 3 to 9%). In addition, by comparing the module 4 and 8 we can notice the effect of the auto shading between the modules themselves. That it is remarkable by looking at the blue and green colors on the module 8 compared to the red one on the module 4 (figure 5) since the latter represent the first row so it's not shaded by another module.

Tab. 1:Solar radiation per module Wh/m2 per module (without obstacle) for the first of January.

Without	Hour=7	Hour=8	Hour=9	Hour=10	Hour=11	Hour=12	Hour=13	Hour=14	Hour=15
Module=1	914	5950	34692	57679	55248	29410	20915	15072	5275
Module=2	909	5073	33972	58102	56190	29981	20960	13019	4733
Module=3	1039	5881	8961	44119	56106	30559	21531	12582	4820
Module=4	1406	7787	8039	17197	45482	29844	21405	13327	4756
Module=5	696	3744	18997	31173	31837	19421	14993	9635	3492
Module=6	693	3844	18870	31113	31829	19420	14943	9410	3439
Module=7	729	4014	6918	24821	32449	20132	15570	9778	3609
Module=8	872	6566	7633	11582	27706	20026	15540	9783	3624
Module=10	737	4099	19282	31674	32738	20355	15708	9858	3652
Module=11	728	4019	6715	24345	32001	19944	15418	9652	3578
Module=12	872	8050	8456	10992	26798	19252	14884	9380	3455
Module=13	717	3955	18778	30740	31499	19340	14956	9519	3499
Module=14	742	4081	19009	31127	32216	20100	15567	9751	3623
Module=15	740	4077	6822	24426	32070	20009	15510	9719	3618
Module=16	941	9800	9874	24436	32277	20331	15813	9903	3704

Tab. 2: Solar radiation per module Wh/m2 per module (with obstacle) for the first of January.

With	Hour=7	Hour=8	Hour=9	Hour=10	Hour=11	Hour=12	Hour=13	Hour=14	Hour=15
Module=1	825	5604	34343	57401	54807	28889	20413	14847	5127
Module=2	808	4667	33535	57737	55616	29398	20459	12834	4623
Module=3	890	5188	8291	43582	55254	28738	20807	12318	4708
Module=4	835	4648	6692	16379	44236	28597	20374	13140	4705
Module=5	611	3449	18701	30949	31537	19157	14767	9571	3455
Module=6	622	3569	18764	31228	32070	19704	15180	9693	3564
Module=7	541	3157	6183	24229	31585	19352	14900	9613	3547
Module=8	457	2520	4686	10460	26120	18585	14375	9515	3551
Module=10	610	3546	18785	31269	32183	19843	15304	9736	3571
Module=11	525	3009	5834	23687	31073	19123	14777	9530	3528
Module=12	417	2194	4050	9553	24848	17509	13504	9022	3346
Module=13	608	3549	18359	30422	31095	18974	14657	9424	3431
Module=14	595	3336	18404	30653	31592	19547	15116	9648	3573
Module=15	514	2865	5581	23640	30990	19042	14727	9518	3523
Module=16	411	2140	3841	22168	29345	17525	13504	9030	3353

- Case2: Real district of Geneva (Carouge); Role of reflective materials.

For this case study, the results are zoomed in a way that we can well visualize and compare the irradiation values between the two simulation. So, two positions are chosen, where one can have vertical and horizontal surfaces. Figure 7,8 and 9 show the irradiation maps of the two simulations (35% and 90% reflective materials) using

Geneva weather file. Some annual irradiation values in kWh/m2, on the zoomed surfaces, are shown in order to compare the result. Comparing these values, we see that by changing the reflective property of the material, we can observe changes in the potential predictions between 7 to 20%. It is clear that the irradiation on roofs, like shown in figure 7,8 and 9 (colored almost in red and orange), represent more solar radiation than the facades but so in an urban area where the presence of these verticals is in large quantities, exploitation leads to a change in solar potential like it was proofed also by (Redweik, Catita, et Brito 2013).

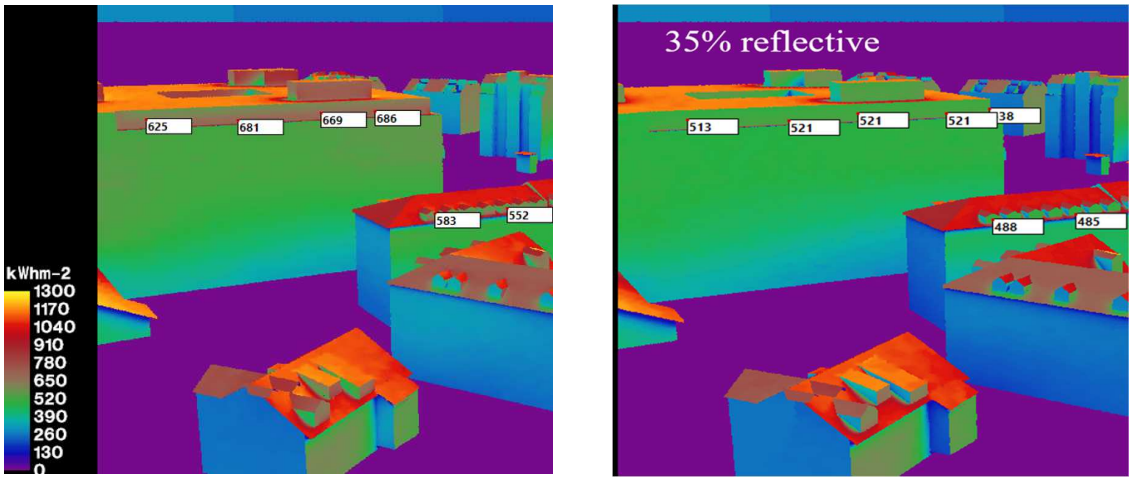

Figure 7: Irradiation map in kWh / m2, 90% and 35%reflective materials

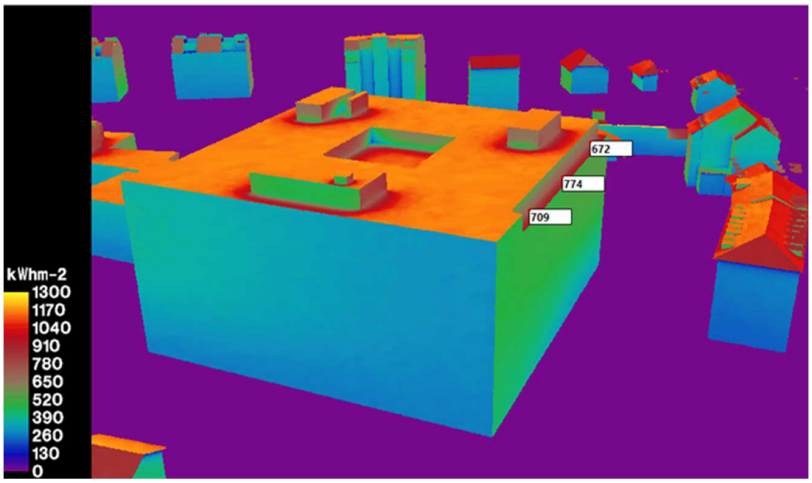

Figure 8:Irradiation map in kWh / m2, 90% reflective materials.

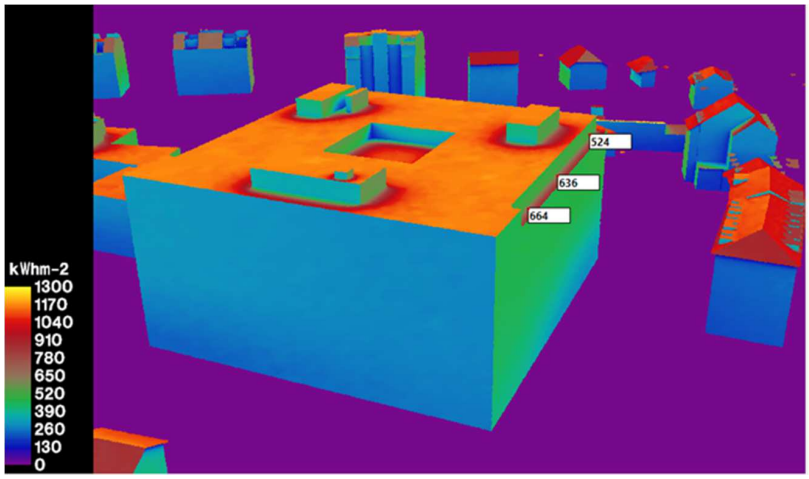

Figure 9:Irradiation map in kWh / m2, 35% reflective materials.

The irradiation values calculated by DIVA included as already said the reflected part of the radiation arriving on a given surface. And thus after comparisons of the results, this increase of irradiation values when the reflecting property increases is rather because of the increase of the reflected radiation on the surface of the buildings coming from the obstacle.

According to these two case studies, between 3% and 50% loss can be achieved because of the addition of obstacle. And up to 20% of irradiation was gained due to the high reflective materials characteristics of building compared to those with low reflective properties.

5. Conclusion /Future Work

Two case studies were performed using DIVA-FOR-RHINO. The first case was a simple case, a region created using Sketchup and then modulated with DIVA. The addition of an obstacle enchains a decrease of solar irradiation arriving on the surface to study. For the second case study, which is carried out on Carouge district in Geneva, the variation in properties of building materials, from 35% reflective up to 90%, results an increase in solar irradiation and so the importance of solar radiation reflected on a given surface is highlighted. The rays reaching surface, are also increasing on the verticals surface and consequently an urban area having numerous facades can have a higher solar potential. For the future work, the same work could be done for several cases (even fictitious ones) for which the density of the obstacles, their height, the reflectivity (unique for all the obstacles then randomly assigned (or not) for each obstacle). In addition, we should add the electrical production using the irradiation values obtained. For the effect of microclimate in solar potential, we have to compare the production profile for temperature data of the nearest meteorological station and the real temperature measured using the UWG program.

6. References

Al Garni, Hassan Z., Anjali Awasthi, et David Wright. 2019. « Optimal orientation angles for maximizing energy yield for solar PV in Saudi Arabia ». *Renewable Energy* 133 (avril): 538-50. https://doi.org/10.1016/j.renene.2018.10.048.

Badescu, V. 2002. « 3D Isotropic Approximation for Solar Diffuse Irradiance on Tilted Surfaces ». *Renewable Energy* 26 (2): 221-33. https://doi.org/10.1016/S0960-1481(01)00123-9.

Bloem, J. J. 2008. « Evaluation of a PV-integrated building application in a well-controlled outdoor test environment ». *Building and Environment*, Outdoor Testing, Analysis and Modelling of Building Components, 43 (2): 205-16. https://doi.org/10.1016/j.buildenv.2006.10.041.

Brito, M. C., S. Freitas, S. Guimarães, C. Catita, et P. Redweik. 2017. « The importance of facades for the solar PV potential of a Mediterranean city using LiDAR data ». *Renewable Energy* 111 (octobre): 85-94. https://doi.org/10.1016/j.renene.2017.03.085.

Bueno, Bruno, Matthias Roth, Leslie Norford, et Reuben Li. 2014. « Computationally efficient prediction of canopy level urban air temperature at the neighbourhood scale ». *Urban Climate* 9 (septembre): 35-53. https://doi.org/10.1016/j.uclim.2014.05.005.

Desthieux, Gilles, Claudio Carneiro, Reto Camponovo, Pierre Ineichen, Eugenio Morello, Anthony Boulmier, Nabil Abdennadher, Sébastien Dervey, et Christoph Ellert. 2018. « Solar Energy Potential Assessment on Rooftops and Facades in Large Built Environments Based on LiDAR Data, Image Processing, and Cloud Computing. Methodological Background, Application, and Validation in Geneva (Solar Cadaster) ». *Frontiers in Built Environment* 4. https://doi.org/10.3389/fbuil.2018.00014.

Hay, John E. 1979. « Calculation of Monthly Mean Solar Radiation for Horizontal and Inclined Surfaces ». *Solar Energy* 23 (4): 301-7. https://doi.org/10.1016/0038-092X(79)90123-3.

Liu, Benjamin, et Richard Jordan. 1960. « The Interrelationship and Characteristic Distribution of Direct, Diffuse and Total Solar Radiation ». *Solar Energy* 4 (juillet): 1-19. https://doi.org/10.1016/0038-092X(60)90062-1.

Lobaccaro, Gabriele, Francesco Fiorito, Gabriele Masera, et Tiziana Poli. 2012. « District Geometry Simulation: A Study for the Optimization of Solar Façades in Urban Canopy Layers ». *Energy Procedia*, 1st International Conference on Solar Heating and Coolingfor Buildings and Industry (SHC 2012), 30 (janvier): 1163-72. https://doi.org/10.1016/j.egypro.2012.11.129.

Morakinyo, Tobi Eniolu, Ahmed Adedoyin Balogun, et Olumuyiwa Bayode Adegun. 2013. « Comparing the effect of trees on thermal conditions of two typical urban buildings ». *Urban Climate* 3 (mai): 76-93. https://doi.org/10.1016/j.uclim.2013.04.002.

Naboni, Emanuele, Jonathan Natanian, Giambattista Brizzi, Pietro Florio, Ata Chokhachian, Theodoros Galanos, et Parag Rastogi. 2019. « A digital workflow to quantify regenerative urban design in the context of a changing climate ». *Renewable and Sustainable Energy Reviews* 113: 109255.

Perez, R., R. Seals, et J. Michalsky. s. d. « All-Weather Model for Sky Luminance Distribution—Preliminary Configuration and Validation ». *Solar Energy* 50 (3): 235-45.

Redweik, P., C. Catita, et M. Brito. 2013. « Solar energy potential on roofs and facades in an urban landscape ». *Solar Energy* 97 (novembre): 332-41. https://doi.org/10.1016/j.solener.2013.08.036.

Yuan, Jihui, Craig Farnham, Kazuo Emura, et Siqiang Lu. 2016. « A method to estimate the potential of rooftop photovoltaic power generation for a region ». *Urban Climate* 17 (septembre): 1-19. https://doi.org/10.1016/j.uclim.2016.03.001.

Zhang, Ji, Le Xu, Veronika Shabunko, Stephen En Rong Tay, Huixuan Sun, Stephen Siu Yu Lau, et Thomas Reindl. 2019. « Impact of urban block typology on building solar potential and energy use efficiency in tropical high-density city ». *Applied Energy* 240 (avril): 513-33. https://doi.org/10.1016/j.apenergy.2019.02.033.